

Polarization Signals of the 21 cm Background from the Era of Reionization

Asantha Cooray and Steven R. Furlanetto

*Theoretical Astrophysics, Division of Physics, Mathematics and Astronomy, California Institute of Technology
MS 130-33, Pasadena, CA 91125. E-mail: (asante,sfurlane)@caltech.edu*

18 November 2017

ABSTRACT

While emission and absorption lines of the 21 cm spin-flip transition of neutral Hydrogen are intrinsically unpolarized, a magnetic field creates left- and right-handed polarized components through the Zeeman effect. Here we consider the resulting polarization of the redshifted 21 cm background from the intergalactic medium before reionization. The polarization is detectable in regions with a strong gradient in the mean brightness temperature. In principle, this can open a new window on the evolution of intergalactic magnetic fields. One possible approach is an extended integration of an individual target during this era, such as the Mpc-scale HII regions inferred to surround quasars at $z \sim 6.5$. The differential intensity between the two polarization states can be used as a probe of the magnetic field at the edge of the HII region. We estimate that the SKA could (ignoring systematics) detect $B \sim 200$ (10) μG coherent over several kiloparsecs with an observational bandwidth of 100 (2) kHz. Beyond individual sources, the statistical properties of wide-field 21 cm polarization maps, such as the angular power spectrum, can be used to constrain the large-scale magnetic field. In this case, the SKA can detect $B \sim 100\mu\text{G}$ fields coherent over many megaparsecs. The magnetic field can be measured in any epoch over which the 21 cm background changes rapidly (for example because the ionized fraction or spin temperature change). Although the resulting constraints with SKA are relatively weak compared to theoretical expectations, they nevertheless offer a unique direct probe of magnetic fields in the high-redshift universe.

Key words: cosmology: theory — diffuse radiation — large scale structure — intergalactic medium

1 INTRODUCTION

The next generation of low-frequency radio interferometers, such as LOFAR and the SKA, is expected to open up the possibility of observing neutral Hydrogen in the intergalactic medium (IGM) at redshifts ~ 10 when the universe transitions from neutral to fully ionized (e.g., Scott & Rees 1990; Madau et al. 1997; Zaldarriaga et al. 2004; Morales & Hewitt 2004) through observations of the redshifted spin-flip transition (with a rest wavelength of 21 cm) against the cosmic microwave background (CMB). This emission (during most of this era) and absorption (at high redshifts if the IGM is cold compared to CMB) is intrinsically unpolarized, so discussions of the 21 cm background from the era of reionization have so far concentrated on measuring the total intensity or brightness temperature and its anisotropies.

While the 21 cm emission is normally unpolarized, a

magnetic field can change that. The Zeeman effect, in general, splits the signal into three parts: an unpolarized central component (π component; Bolton & Wild 1957) bracketed in energy by two polarized components (σ components). When viewed parallel to the magnetic field, the central component disappears and the two σ components are right- and left-handed circularly polarized, respectively. The difference in polarization states occurs because states split by the Zeeman effect have $\pm\hbar$ momenta and, in order to conserve the total angular momentum, the two photons must also be polarized in opposite directions. Polarization of the 21 cm line has been successfully observed and used to determine the magnetic field strength of the interstellar medium (Verschuur 1968; Verschuur 1969) and that towards specific HI features (Verschuur 1995; Verschuur 1989) in the Milky Way, among other applications.

Observations of the polarized 21 cm background from

high redshifts have two applications: (1) the direct determination of the magnetic field strength in isolated regions containing neutral Hydrogen, such as the edges of HII regions around quasars at $z \gtrsim 6$, and (2) the statistical determination of large-scale magnetic field properties (such as its rms fluctuations) during the era of reionization. We shall see that the technique is most powerful when the mean brightness temperature of the 21cm line changes rapidly with frequency, for example because of sharp gradients in the ionized fraction or because of an overall heating of the neutral gas.

This technique thus offers the potential to constrain the IGM magnetic field on a wide range of scales. At present, measurements of Faraday rotation against background quasars constrains the IGM magnetic field to be $\lesssim 10$ nG at $z \sim 0$, if we assume a coherence length of ~ 1 Mpc (see Kronberg 1994 for a review), but it could be larger if the field were tangled on small scales. Assuming flux conservation, this would imply $B \lesssim ([1+z]/7)^2 \mu\text{G}$, if the coherence length remained 1 Mpc comoving. Within galaxies and galaxy clusters, field strengths are typically $\sim 1\text{--}100 \mu\text{G}$ with coherence lengths of $\lesssim 10$ kpc (e.g., Clarke et al. 2001 and references therein). The origin of these fields is uncertain. Early-universe processes can generate extremely weak seed fields on small scales (Quashnock et al. 1989). Fields can be amplified during the formation of galaxies through the dynamo process (Kulsrud 1999), but such a process will not work on the large scales of galaxy clusters (or the IGM). Seed fields could also be generated during reionization itself (Gnedin, Ferrara, & Zweibel 2000). A more promising possibility is for quasar or supernova winds to entrain the fields and carry them into the IGM (Kronberg et al. 1999, 2001; Furlanetto & Loeb 2001; Gopal-Krishna & Wiita 2001). Measurements of the field strength at $z \gtrsim 6$ could offer invaluable insight into these processes: because structure formation is much less advanced, galaxies and quasars should have polluted much less of the universe. However, placing such constraints promises to be difficult. For example, the number of bright sources available for Faraday rotation observations is probably quite small, and the rotation may be dominated by the low-redshift universe because of the much larger path length. The polarized 21 cm background presents an alternate possibility; although we shall see that the constraints are fairly weak compared to most magnetic field generation scenarios, they are still the most promising direct measurements for the high-redshift universe.

The discussion is organized as follows: in § 2, we discuss the polarized 21 cm signal and consider two separate applications involving individual targets (§ 2.1) and large-scale statistics (§ 2.2). In the same sections, we also discuss the potential detectability of these signatures with upcoming low-frequency radio telescopes arrays such as the SKA. We conclude with a summary in § 3. Throughout the paper, we make use of the WMAP-favored ΛCDM cosmological model (Spergel et al. 2003).

2 METHOD OF CALCULATION

In the presence of a magnetic field, the Zeeman effect causes a level splitting of the 21 cm line with magnitude $\delta\nu \equiv$

$|\nu - \nu_0|$ (Lang 1999) such that

$$\begin{aligned} \nu &= \nu_0 \pm \frac{eB}{4\pi m_e c} \\ &= 1420 \text{ MHz} \pm 14 \text{ Hz} \left(\frac{B}{10 \mu\text{G}} \right). \end{aligned} \quad (1)$$

For typical magnetic fields of order $\sim 10 \mu\text{G}$, the fractional separation of the two states is significantly smaller than the line width of the 21 cm emission (typically many kHz or more). Thus, observing two separate peaks in the line profile is not possible. The polarization of these two states, however, is a potentially measurable quantity if the magnetic field strength is such that the magnitude of the difference between left- and right-handed polarization is larger than the detector noise.

We denote the magnetic field parallel to the line of sight as $B_{\parallel} = \hat{\mathbf{n}} \cdot \mathbf{B}$. We then write the total brightness temperature and the difference in the brightness temperature between left- and right-handed polarization maps as:

$$\begin{aligned} \Delta T_{\text{tot}}(\nu) &= \Delta T_L(\nu) + \Delta T_R(\nu) \\ \Delta P_{\text{diff}}(\nu) &= |\Delta T_L(\nu) - \Delta T_R(\nu)|. \end{aligned} \quad (2)$$

The difference term can be simplified because $\Delta T_L(\nu) \propto \Delta T_{\text{tot}}(\nu_0 - \delta\nu)$ while $\Delta T_R(\nu) \propto \Delta T_{\text{tot}}(\nu_0 + \delta\nu)$, as the two states separated in frequency are also polarized in opposite directions. Thus

$$\begin{aligned} \Delta P_{\text{diff}}(\nu) &= 2 \frac{d\Delta T_{\text{tot}}}{d\nu}(\nu) \delta\nu \\ &= 28 \Delta T'_{\text{tot}}(\nu) \left(\frac{\hat{\mathbf{n}} \cdot \mathbf{B}}{10 \mu\text{G}} \right), \end{aligned} \quad (3)$$

where $\Delta T'_{\text{tot}}(\nu)$ is the derivative of the emission profile with respect to the frequency (in Hz). Polarization observations have the advantage that, although $\delta\nu$ is extremely small, one can still constrain magnetic field with an observed bandwidth significantly larger than $\delta\nu$, so long as the gradient $\Delta T'_{\text{tot}}$ over that frequency range is large.

During the era of reionization, there are two distinct possibilities for polarization observations: (a) individual targets, such as HII regions surrounding $z \sim 6$ quasars, and (b) maps of the high- z universe as a whole. We will first discuss the extent to which magnetic fields in individual quasar regions can be measured with first-generation 21 cm interferometers, such as LOFAR and the SKA and then discuss applications of statistical studies with wide-field maps of the 21 cm background.

2.1 Individual HII Regions

It is now widely believed that the reionization process was both inhomogeneous and patchy on large scales (Barkana & Loeb 2001; Furlanetto, Zaldarriaga, & Hernquist 2004a). Luminous sources such as the first galaxies and quasars ionized their surroundings and these ionized patches grew and overlapped until they completely ionized the universe. These ionized patches contribute to CMB temperature (Santos et al. 2003) and polarization anisotropies (Zaldarriaga 1997), cause fluctuations in the 21 cm background (Furlanetto, Zaldarriaga, & Hernquist 2004b), and correlate the two (Cooray

2004a,b). The reionization process was not instantaneous (Wyithe & Loeb 2003; Cen 2003; Chen et al. 2003; Haiman & Holder 2003) and could, in certain models, explain both the high electron scattering optical depth $\tau_{\text{es}} = 0.17 \pm 0.04$ measured through the large angular scale bump in the CMB temperature-polarization cross-correlation (Kogut et al. 2003) and the rapidly evolving neutral fraction x_H at $z \sim 6$ towards Sloan Digital Sky Survey quasars (Fan et al. 2002). During the partially ionized phase, each high- z quasar should be surrounded by an HII region expanding into a largely neutral medium, with its size determined by the quasar luminosity and spectrum (Wyithe & Loeb 2004b, Mesinger & Haiman 2004).

While 21 cm intensity observations of these sources could reveal the shape of these HII regions, especially in combination with Ly α optical depth profiles (Wyithe & Loeb 2004b), polarization measurements can reveal the presence of a magnetic field. To estimate the expected polarization signal, we only need the width of the edge of the HII region (which determines $\Delta T'_{\text{tot}}(\nu)$ in eq. [3]). This is determined by the mean free path λ of an ionizing photon, which in turn depends on the photon energy (and hence the quasar spectrum). Using a typical quasar spectrum, Wyithe & Loeb (2004b) estimate $\lambda \sim 1.5x_H^{-1}(1+z)^{-3}$ Mpc (proper). This corresponds to a frequency width of $\Delta\nu_{\text{HII}} \sim 2$ kHz, much smaller than the resolution of any of the upcoming experiments. This is only a rough estimate given uncertainties in the exact shape of the quasar UV spectrum and the physical state of the IGM surrounding these quasars, but it suffices for simple estimates of the signal.

Using the above case as an example, we estimate polarized signals of order $\Delta P_{\text{diff}} \sim 0.3\text{mK}(B_{\parallel}/10\mu\text{G})$ if the observed bandwidth $\Delta\nu_{\text{ch}}$ exceeds $\Delta\nu_{\text{HII}}$. Of course, only the transition region produces polarized flux, so the fractional polarization is $\sim (\Delta\nu_{\text{HII}}/\Delta\nu_{\text{ch}})(\Delta P_{\text{diff}}/\Delta T_{\text{tot}}) \sim 0.03\%$ for $\nu_{\text{ch}} = 0.1$ MHz. Note that this assumes a field coherent across the several kiloparsec thickness of the transition region; field reversals (either in frequency space or across the telescope beam) would cause the net polarization to execute a random walk and weaken the limit. This weak signal presents a substantial challenge for an unambiguous detection given the large number of systematics in these measurements. Nevertheless, with the rapid improvement in technology and the unknown astrophysical environment (which could potentially increase the amplitude of polarized components), it is useful to estimate the level of magnetic fields detectable by future instruments.

We let $N_{\Delta\nu_{\text{ch}}}$ be the rms noise in each polarization component over a bandwidth $\Delta\nu_{\text{ch}}$. The minimum detectable magnetic field strength (parallel to the line of sight), at the signal-to-noise level of unity, is then

$$B_{\parallel}^{\text{min}} (\mu\text{G}) = \frac{\sqrt{2}N_{\Delta\nu_{\text{ch}}}}{2.8\Delta T'_{\text{tot}}(\nu)[\Delta\nu_{\text{HII}}/\Delta\nu_{\text{ch}}]}. \quad (4)$$

The factor $\sqrt{2}$ accounts for the fact that the measurement is a difference between polarizations. The bandwidth factor appears because the signal contributes to only a fraction of the channel (we have assumed $\Delta\nu_{\text{ch}} \geq \Delta\nu_{\text{HII}}$ here). The root

mean square noise contribution in a single SKA¹ channel is

$$N_{\Delta\nu} = 0.079\text{mK} \left(\frac{203\text{MHz}}{\nu} \right)^2 \left(\frac{A_{\text{eff}}/T_{\text{sys}}}{2 \times 10^4 \text{m}^2 \text{K}^{-1}} \right)^{-1} \\ \times \left(\frac{4'}{\Delta\theta} \right)^2 \left(\frac{0.1\text{MHz}}{\Delta\nu_{\text{ch}}} \frac{30\text{days}}{t_{\text{int}}} \right)^{1/2}, \quad (5)$$

where $A_{\text{eff}}/T_{\text{sys}}$ captures the sensitivity of an array with a collecting area of A_{eff} and a system temperature T_{sys} , $\Delta\theta$ is the beam size, and t_{int} is the total integration time. The parameters are for the straw-man SKA, with revised values scaled from the estimate in Zaldarriaga et al. (2004). In one month of continuous integration, SKA can reach noise levels of $\sim 80 \mu\text{K}$ with these parameters, so one could potentially limit the magnetic field to a level of $\sim 200 \mu\text{G}$ at the one-sigma level. If we reduce the bandwidth to $\Delta\nu_{\text{ch}} = 10$ (2) kHz centered on the edge of the HII region, the one-sigma constraint is ~ 60 (9) μG . While smaller bandwidths are desirable, resulting increase in systematics complicate such an observation. Narrow channels of order 2 kHz are also limited by the curvature of the HII region across the beam (which would cause the edge to move in frequency space). The latter could be avoided by careful binning of smaller pixels.

Thus, for a reasonable bandwidth, the expected SKA limit is significantly higher than many of the theoretical expectations at these redshifts. Models in which quasar outflows or starburst winds pollute the IGM usually have an average field strength of $\sim 1\mu\text{G}$ in the magnetized regions (e.g. Furlanetto & Loeb 2001) and primordial magnetic fields are expected to be much weaker. Reaching a $\sim 1 \mu\text{G}$ detection level would require an order of magnitude increase in sensitivity relative to SKA and a better control of systematics such that observations can be made over a bandwidth of a few kHz level. However, it is important to note that strengths of $\sim 1\mu\text{G}$ are only average levels. The fields could vary spatially within magnetized regions, especially near galaxies and quasars. Because the edge of the HII regions are several kpc thick, this test would be sensitive to any strong fields tangled on these scales.

2.2 Anisotropy Studies

In addition to individual targets, one can also measure polarization statistics with wide-field maps. This is analogous to proposed measurements of the 21 cm power spectrum (Zaldarriaga et al. 2004), and we take a similar approach to describing the polarized visibilities.

In the case of polarization, we write the multipole moments of a difference map of the two orthogonal states as

$$a_{lm}^{\text{diff}} = \int d\hat{\mathbf{n}} \Delta P_{\text{diff}}(\hat{\mathbf{n}}) Y_l^{m*}(\hat{\mathbf{n}}), \quad (6)$$

where $\Delta P_{\text{diff}}(\hat{\mathbf{n}})$ is now the difference in maps when observations have integrated over a finite bandwidth such that

¹ <http://www.skatelescope.org> for details

$$\Delta P_{\text{diff}}(\hat{\mathbf{n}}) = 2.8 \int dr \Delta T'_{\text{tot}}(\hat{\mathbf{n}}r, r) [\hat{\mathbf{n}} \cdot \mathbf{B}(\hat{\mathbf{n}}r, r)] W_\nu(r). \quad (7)$$

Here the magnetic field is measured in units of μG , r is the comoving distance, and $W_\nu(r)$ describes the experimental response, assumed to peak at a distance r_0 . The window function thus picks out a particular redshift interval because the 21 cm feature is a spectral line. We take the response function to be a Gaussian of width $\Delta\nu_{\text{ch}}$. The frequency derivative can also be transformed to a function of redshift via $d\Delta T(z)/d\nu = -\nu_0/\nu^2 d\Delta T(z)/dz$, where ν is the observed frequency, $\nu = \nu_0(1+z)^{-1}$.

The maximum magnitude is set by the overall strength of the 21 cm intensity. Following Zaldarriaga et al. (2004), the mean brightness temperature of the 21 cm line is

$$\Delta T^{21\text{cm}}(z) = 23.2 \text{ mk} \left(\frac{\Omega_b h^2}{0.02} \right) x_H(z) \left[\frac{T_S - T_{\text{CMB}}}{T_S} \right] \sqrt{1+z}, \quad (8)$$

where $T_{\text{CMB}} = 2.73(1+z)$ K is the CMB temperature at redshift z and T_S is the gas spin temperature. Henceforth for simplicity we will neglect spatial fluctuations in T_S and x_H (though we will allow both to be functions of redshift). The angular power spectrum of the polarization difference map includes fluctuations both in the neutral Hydrogen density field (which are captured by eq. [8]) and spatial fluctuations of the magnetic field. With our approximation, fluctuations in the density cause $\delta T(\hat{\mathbf{n}}) = \Delta T^{21\text{cm}}(\hat{\mathbf{n}})[1 + \delta_g(\hat{\mathbf{n}})]$, where $n_H = \bar{x}_H \bar{n}_g(1 + \delta_g)$, the mean baryonic density of the universe is \bar{n}_g , and the mean neutral fraction is \bar{x}_H . They can thus be encapsulated in $P_{gg}(k)$, the spatial power spectrum of gas density fluctuations (with respect to the mean density). The remaining term depends on $P_{BB}(k)$, the spatial power spectrum of the magnetic field (which we will measure in absolute units of $\mu\text{G}^2 \text{Mpc}^{-3}$). The relation between the two power spectra is currently unknown. It is possible that the coherence scale of the magnetic field is larger than that of the density field (this is similar to the the velocity field, which has a larger correlation length than the density field). On the other hand, the opposite situation could apply if magnetic fields are highly tangled.

In either case, the power spectrum may then be written

$$C_l^{\text{diff}} = \int \frac{dr}{d_A^2} \left[2.8 \frac{d\Delta T^{21\text{cm}}}{dz} \frac{\nu_0}{\nu^2} \right]^2 I\left(\frac{l}{d_A}; r\right) W_\nu(r)^2 \quad (9)$$

in the Limber approximation appropriate for a flat sky (Limber 1954). Here the mode coupling integral I is a convolution between fluctuations in the gas density field and the magnetic field, weighted by a geometric term involving the line of sight angle,

$$I(k) = \int k_1^2 \frac{dk_1}{8\pi^2} \int_{-1}^{+1} d\mu \frac{(1-\mu^2)}{y_2^2} P_{gg}(ky_2) P_{BB}(ky_1), \quad (10)$$

where $y_1 = k_1/k$ and $y_2 = k_2/k = \sqrt{1 - 2\mu y_1 + y_1^2}$. This form for the power spectrum occurs because equation (7) presents a convolution between the frequency derivative of the mean brightness temperature and fluctuations in the line-of-sight magnetic field. The same formula can also be derived as an overall modulation of the mean brightness

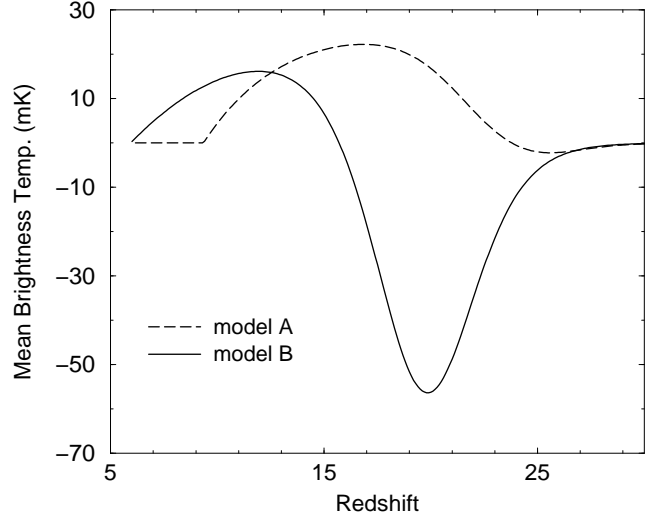


Figure 1. Mean brightness temperature as a function of the redshift for two different models of the reionization history. In model A (dashed line), we have $\zeta = 20$, $f_\star = 0.05$, and $f_{\text{heat}} = 1$. Here heating occurs early and $\Delta T^{21\text{cm}}$ traces \bar{x}_H for $z \lesssim 15$. Model B (solid line) has $\zeta = 6$, $f_\star = 0.03$, and $f_{\text{heat}} = 0.01$. Heating is much less rapid in this case, but $\Delta T^{21\text{cm}}$ still traces \bar{x}_H for $z \lesssim 11$.

temperature by fluctuations in the magnetic field and, in this sense, the derivation is analogous to calculations in the literature (e.g., Cooray 2001) of the Ostriker & Vishniac (1987) effect, which is a modulation of the density field by the velocity fluctuations.

In the limit in which small-scale fluctuations in the brightness temperature (from density structure) modulate a more coherent magnetic field, $k_2 = |\mathbf{k} - \mathbf{k}_1| \sim k$ such that $y_1 \ll 1$ and $y_2 \rightarrow 1$. Thus, $I(k) \rightarrow P_{gg}(k) \int k_1^2 dk_1 / 2\pi^2 P_{BB}(k_1) \int_{-1}^{+1} d\mu (1 - \mu^2) / 4$. The integral over μ simplifies to $1/3$ such that $I(k) \rightarrow P_{gg}(k) B_{\text{rms}}^2(r) / 3$, where

$$B_{\text{rms}}^2 = \int \frac{k^2 dk}{2\pi^2} P_{BB}(k). \quad (11)$$

Thus, if the magnetic field is spatially uniform on larger scales than the density fluctuations, we have

$$C_l^{\text{diff}} = \int \frac{dr}{d_A^2} \left[2.8 \frac{d\Delta T^{21\text{cm}}}{dz} W_\nu(r) \right]^2 P_{gg}\left(\frac{l}{d_A}; r\right) \frac{B_{\text{rms}}^2(r)}{3}. \quad (12)$$

In this case, the factor $1/3 B_{\text{rms}}^2$ can also be understood as a random averaging when the two line of sight angles are nearly parallel (i.e. the small angle approximation):

$$\langle [\hat{\mathbf{n}} \cdot \mathbf{B}(r_1)] [\hat{\mathbf{n}}' \cdot \mathbf{B}(r_2)] \rangle \approx \frac{1}{3} \langle B^2 \rangle. \quad (13)$$

We will now restrict ourselves to the simple limiting case of eq. (12) appropriate for large-scale magnetic fields. To proceed, we need a model for $d\Delta T/dz$. This has three components: the cosmological density evolution, \bar{x}_H , and T_S . We compute \bar{x}_H following Furlanetto et al. (2004a), who assume that the ionized fraction is proportional to the collapse

fraction (with a constant ζ , part of which is determined by the star formation efficiency f_*). The spin temperature evolution is more subtle. At these redshifts, T_S is coupled to the gas kinetic temperature by Ly α photons (Field 1959; Madau et al. 1997). We follow this background in the same way as Ciardi & Madau (2003), assuming that five photons are produced near Ly α for every ionizing photon, as appropriate for Population II stars with a constant star formation (see their Fig. 1). We assume that the IGM cools adiabatically after decoupling from the CMB. We then heat it through X-rays from supernovae inside the ionizing sources. We assume one supernova occurs per $100 M_\odot$ of stars and that each has 10^{51} ergs. We further assume that a fraction f_{heat} of the supernova energy escapes into X-rays and uniformly heats the IGM. Fig. 1 illustrates two models. Model A is a ‘maximal heating’ scenario in which $\Delta T^{21\text{cm}}$ rises rapidly and decreases later only through reionization. Model B is a ‘minimal heating’ scenario in which the IGM remains cool for a long period but still emits well before reionization occurs. Neither of these models can be taken as more than a representative possibility, as they neglect a number of important effects (such as shock heating in the IGM, other X-ray sources, and a rigorous treatment of the Ly α background), but they suffice for the purposes of estimating the brightness temperature gradients for our calculation.

In Fig. 2, we show the polarization and temperature angular power spectra for model B at $z = 9$. In these calculations, we describe the density power spectrum with the linear density field, but scaled by a bias factor appropriate to the distribution of neutral Hydrogen (Mo et al. 1997). Specifically, we follow the methods of Santos et al. (2003, 2004), who use an approach similar to halo models of large scale structure (Cooray & Sheth 2002). We also show noise curves for the SKA and for an ‘extended SKA’. The polarized signal is proportional to the brightness temperature gradient. We have chosen a point at which this is relatively shallow in Fig. 1; if the rapid temperature evolution of model B at $z \sim 15\text{--}25$ is accessible to observations, the polarized signal could be a few times larger. The signal for the late stages of reionization in model A would be comparable to that shown in Fig. 2. Moreover, we have assumed a uniform \bar{x}_H ; spatial variations in the ionized fraction (or in T_S) could also increase the signal by a factor of a few. On the other hand, we have neglected possible correlations between the density and the magnetic field, and we have neglected small-scale structure in B . Our estimate can therefore only be taken as a guide to the expected order of magnitude of the signal.

We can estimate the smallest detectable B_{rms} using the Fisher matrix approach. Since only a single parameter is involved, we can write the limit on the magnetic field as simply

$$\sigma^{-2}(B_{\text{rms}}) = \sum_l \frac{1}{(\sigma_l^{\text{diff}})^2} \left(\frac{\partial C_l^{\text{diff}}}{\partial B_{\text{rms}}} \right)^2, \quad (14)$$

where

$$\sigma_l = \sqrt{\frac{2}{(2l+1)f_{\text{sky}}}} (C_l^{\text{diff}} + C_l^{\text{noise}}), \quad (15)$$

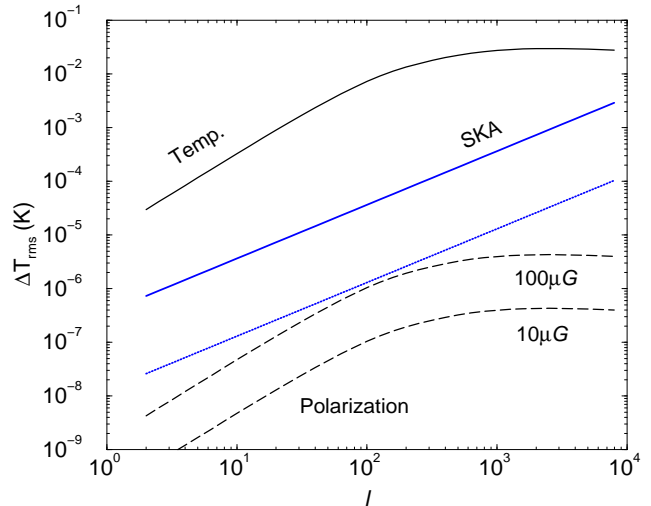


Figure 2. The rms brightness temperature fluctuations of the 21 cm background at $z = 9$ ($\nu_{\text{obs}} = 142$ MHz), where $\Delta T_{\text{rms}} = \sqrt{l(l+1)}C_l/2\pi$. The top solid curve (labeled ‘Temp.’) shows the total temperature fluctuations, while the long-dashed curves show the fluctuations in the polarization difference assuming a large scale magnetic field with $B_{\text{rms}} = 10$ and $100\mu\text{G}$. Both assume model B of Fig. 1. The ‘SKA’ curve shows the instrumental noise, unbinned in the multipole space, for a one month integration with $\Delta\nu_{\text{ch}} = 0.5\text{MHz}$. The bottom (linear) curve assumes an order of magnitude improvement in sensitivity over the SKA, a year-long integration, and a total bandwidth of 8 MHz.

with f_{sky} the fraction of sky observed and C_l^{noise} the instrumental noise. We make the null hypothesis $C_l^{\text{diff}} = 0$ and estimate the one-sigma constraint on B_{rms} for the two different noise curves shown in Fig. 2. For the standard SKA noise parameters with a one month observation, we find $B_{\text{rms}} \geq 224(f_{\text{sky}}/0.1)^{-0.5} \mu\text{G}$ is detectable (at 1σ). With an order of magnitude improved sensitivity and a year-long observation, the limit improves to $B_{\text{rms}} \geq 7.5(f_{\text{sky}}/0.1)^{-0.5} \mu\text{G}$. As with targeted observations of HII regions, it is thus difficult to probe the μG fields expected from many models. Long integrations with instruments beyond the SKA will be required to reach the necessary limits.

3 SUMMARY

While emission (and absorption) from the 21 cm spin-flip transition of neutral Hydrogen is intrinsically unpolarized, a magnetic field creates left- and right-handed polarization through the Zeeman effect. For individual targets of neutral Hydrogen during the era of reionization, such as Mpc-scale HII regions surrounding quasars at $z \gtrsim 6$, the difference in intensity between these two polarization states can be used as a probe of the magnetic field on the scale of the edge of the HII region. For example, observations of the known SDSS quasars at $z \sim 6.5$ with the SKA can constrain magnetic fields to a level of $200 \mu\text{G}$ (at the 1σ level) in an integration of one month over a bandwidth of 100 kHz. If a few kHz bandwidth observations can be made with systematics well

under control, the limit improves to $\sim 10 \mu\text{G}$, again at the 1σ level. The expected fields have $B \lesssim 3\mu\text{G}$ so one could potentially reach an interesting constraint through a long integration or an even larger instrument. In addition, these measurements are sensitive to fields with scales of several kpc, which could be much larger than the mean value.

Beyond individual sources, the statistical properties of 21 cm polarization in wide-field maps, such as the angular power spectrum of fluctuations, can also be used to constrain large scale fluctuations of the magnetic field. This requires the mean brightness temperature of the 21 cm background to vary rapidly as a function of the frequency. Thus polarization detections are limited to epochs over which the underlying properties of the 21 cm background, such as the ionized fraction and spin temperature, change rapidly. Using simple models for the evolution of the mean brightness temperature, we have estimated the statistical constraints that can be placed on a magnetic field coherent over scales larger than that of the density field for such a measurement. The SKA can detect a large-scale field with $B_{\text{rms}} \geq 224(f_{\text{sky}}/0.1)^{-0.5} \mu\text{G}$. A future instrument with an order of magnitude better sensitivity can improve the limit to $B_{\text{rms}} \geq 7.5(f_{\text{sky}}/0.1)^{-0.5} \mu\text{G}$ with a year-long observation. Constraints of this order would be desirable given that galaxy clusters at $z \lesssim 1$ are known to have $B_{\text{rms}} \sim 10\text{--}100\mu\text{G}$ (e.g., Clarke et al. 2001).

Finally, we emphasize that, although the limits obtainable from the 21 cm background are weak compared to theoretical expectations, obtaining other direct constraints on the magnetic field during the era of reionization promises to be equally challenging. This technique may offer the first direct limits on high-redshift magnetic fields.

Acknowledgments: This work was supported at Caltech by a Senior Research Fellowship from the Sherman Fairchild foundation. We thank John Kovac for useful discussions.

REFERENCES

- Barkana, R. & Loeb, A. 2001, *Physics Reports*, 349, 125
 Bolton J. G., Wild J. P. 1957, *ApJ*, 125, 296
 Cen R. 2003, *ApJ*, 591, L5
 Chen, X., Cooray, A., Yoshida, N., & Sugiyama, N. 2003, *MNRAS*, 346, L31
 Ciardi, B. & Madau, P. 2003, *ApJ*, 596, 1
 Clarke, T. E., Kronberg, P. P., & Böhringer, H. 2001, *ApJ*, 547, L111
 Cooray A. 2001, *PRD*, 64, 063514
 Cooray A. 2004a, *PRD*, 70, 023508
 Cooray A. 2004b, *PRD*, in press (astro-ph/0405528)
 Cooray, A. & Sheth, R. 2002, *Phys. Rep.*, 372, 1 (astro-ph/02064508)
 Fan X., Narayanan V. K., Strauss M. A., White R. L., Becker R. H., Pentericci L., Rix H. W. 2002, *AJ*, 123, 1247
 Field, G. B. 1959, *ApJ*, 129, 536
 Furlanetto S. R., Loeb A., 2001, *ApJ*, 556, 619
 Furlanetto S. R., Zaldarriaga M., Hernquist L. 2004a, *ApJ*, in press (astro-ph/0403697)
 Furlanetto S. R., Zaldarriaga M., Hernquist L. 2004b, *ApJ*, in press (astro-ph/0404112)
 Gnedin, N. Y., Ferrara, A., & Zweibel, E. G. 2000, *ApJ*, 539, 505
 Gopal-Krishna & Wiita, P. J. 2001, *ApJ*, 560, L115
 Haiman, Z., & Holder, G. P. 2003, *ApJ*, 595, 1
 Kogut A., Spergel D. N., Barnes C., Bennett C. L., Halpern M., Hinshaw G., Jarosik N., Limon M., Meyer S. S., Page L. et al. 2003, *ApJS*, 148, 161
 Kronberg, P. P. 1994, *Prog. Phys.*, 57, 325
 Kronberg, P. P., Lesch, H., & Hopp, U. 1999, *ApJ*, 511, 56
 Kronberg P. P., Dufton Q. W., Li H., Colgate S. A. 2001, *ApJ*, 560, 178
 Kulsrud, R. M. 1999, *ARA&A*, 37, 37
 Lang, K. R. 1999, *Astrophysical Formulae Vol. I*, Springer-Verlag.
 Limber, D. 1954, *ApJ*, 119, 655
 Madau, P., Meiksin, A., & Rees, M. J. 1997, *ApJ*, 475, 429
 Mesinger, A. & Haiman, Z. 2004, *ApJ*, 611, L69
 Mo, H. J., Jing, Y. P., White, S. D. M. 1997, *MNRAS*, 284, 189
 Morales, M. F. & Hewitt, J. 2003, *ApJ*, submitted, astro-ph/0312437
 Ostriker J. P., Vishniac E. T. 1986, *ApJ*, 306, L51
 Quashnock, J. M., Loeb, A., & Spergel, D. N. 1989, *ApJ*, 344, L49
 Santos, M. G., Cooray, A., Haiman, Z., Knox, L., & Ma, C.-P. 2003, *ApJ*, 598, 756
 Santos, M. G., Cooray, Knox L. 2004, in preparation
 Scott, D., & Rees, M. J. 1990, *MNRAS*, 247, 510
 Spergel, D. N., et al. *ApJS*, 148, 175
 Verschuur G. L. 1968, *PRL*, 21, 775
 Verschuur G. L. 1969, *ApJ*, 156, 861
 Verschuur G. L. 1989, *ApJ*, 339, 163
 Verschuur G. L. 1995, *ApJ*, 451, 624
 Wyithe J. S. B., Loeb A. 2003, *ApJ*, 588, L69
 Wyithe J. S. B., Loeb A. 2004a, *Nature*, 427, 815
 Wyithe J. S. B., Loeb A. 2004b, *ApJ*, 610, 117
 Zaldarriaga, M., 1997, *PRD*, 55, 1822
 Zaldarriaga, M., Furlanetto, S. R., Hernquist, L. 2004, *ApJ*, 608, 622